Journal of
Materials Chemistry B

ccepted Manuscript

This article can be cited before page numbers have been issued, to do this please use: . ERUCAR and S. Keskin, *J. Mater. Chem. B*, 2017, DOI: 10.1039/C7TB01764B.

View Article Online
DOI: 10.1039/C7TB01764B

Computational Investigation of Metal Organic Frameworks for Storage and Delivery of Anticancer Drugs

Ilknur Erucar[a] and Seda Keskin[b]*

[a]Department of Natural and Mathematical Sciences, Faculty of Engineering, Ozyegin University, Cekmekoy, 34794, Istanbul, Turkey

[b]Department of Chemical and Biological Engineering, Koc University, Rumelifeneri Yolu, Sariyer, 34450, Istanbul, Turkey

*Corresponding author. E-mail: skeskin@ku.edu.tr Phone: +90 (212) 338-1362

Submitted to Journal of Materials Chemistry B

Abstract

Metal organic frameworks (MOFs) have been recently used in biomedical applications such as drug storage and drug delivery due to their large surface areas, high pore volumes, tunable physical and chemical characteristics. In this study, we investigated MOF-74 materials for efficient storage and delivery of two anticancer drug molecules, methotrexate (MTX) and 5-fluorouracil (5-FU). We initially compared results of our molecular simulations with available experimental data for MTX and 5-FU uptakes of various MOFs. Motivated from the good agreement between experiments and simulations, we computed MTX and 5-FU uptakes in 10 different MOF-74 materials having various physical and chemical properties. At low fugacity, MTX adsorption is favored over 5-FU since MTX has stronger interactions with the MOFs whereas at high fugacity, 5-FU adsorption is favored over MTX due to the entropic effects. Our results showed that MOF-74 materials outperform MTX and 5-FU storage capacities of traditional materials such as polymeric nanoparticles and two dimensional layered nanomaterials. We also examined diffusion of drug molecules in MOFs considering both single-component and mixture transport for the first time in the literature. Both drug molecules diffuse slowly in MOFs suggesting that MOF-74 materials are strong alternatives to traditional porous materials for delivery of MTX and 5-FU. This computational study will be useful to effectively identify the most promising MOFs for target drug delivery applications prior to experiments. Our results will also guide the experiments for design and development of MOFs as anticancer drug carrier systems.

Keywords: metal organic frameworks, methotrexate, 5-fluorouracil, molecular simulations, drug storage, drug delivery.

1. Introduction

Combination therapy, simultaneous administration of two or more therapeutic agents, has been recently used in cancer treatments.[1] The aims are to increase the therapeutic index of drugs and to reduce the side effects and toxicity by using synergistic combinations of drug molecules. Drug delivery systems require a carrier material which can store and deliver optimal doses of drugs. These systems should be able to provide better drug solubility, sustained drug release kinetics and minimized side effects compared to the direct drug administration.[2] A large variety of materials such as copolymeric nanomicelles,[3] liposomes,[4] two dimensional layered nanomaterials,[5] and mesoporous silica[6] has been used as drug carriers. Metal complexes have been also considered for different biomedical applications including drug storage and delivery,[7] bioimaging[8, 9] and chemosensors for protein biomarkers.[10] Among these materials, two dimensional layered nanomaterials such as layered double hydroxide (LDH) and copolymeric nanomicelles of poly-lactic-co-glycolic acid (PLGA) have been investigated as potential multi-drug carriers for cancer treatment.[3, 5] However, low drug loading capacities, rapid drug release, toxicity and economic considerations are the main challenges which limit practical applications of these conventional drug delivery systems. Development of new materials that can efficiently store and deliver multi-drug molecules is strongly needed.

Metal organic frameworks (MOFs) are crystalline porous materials that have received significant attention in the past decade due to their unique properties such as large surface areas (500-6000 m^2/g), high porosities (up to 90% free volume) and a wide range of pore sizes (1-98 Å).[11] Structural and chemical properties of MOFs can be tuned during their synthesis for a target application. MOFs are recently considered for biomedical applications.[7] Due to their high pore volumes, tunable structures and sufficient stability profiles under physiological conditions, MOFs have been accepted as strong candidates for storage and controlled delivery of drug molecules.[12] Initial studies focused on storage of an analgesic and anti-inflammatory drug, ibuprofen, in MOFs. Ibuprofen was encapsulated within the cavities of mesoporous rigid chromium carboxylate MOFs, MIL-100(Cr) and MIL-101(Cr).[13] Results showed that MIL-101(Cr) has very high ibuprofen loading (1.4 g/g MOF), outperforming traditional drug carriers such as zeolite (FAU) (0.16 g/g material) and mesoporous silica (MCM-41) (0.34 g/g material).[14] In a following study, ibuprofen molecule was encapsulated in MIL-53(Fe) and (Cr) materials and an uptake of 0.2 g/g was found in both materials.[15] An et al.[16] synthesized a biocompatible MOF, bio-MOF-1 and showed that it has promise for storage and release of

procainamide. Procainamide loading was determined as 0.22 g/g MOF and controlled release of procainamide was observed due to the ionic interactions between procainamide and bio-MOF-1.

MOFs have been recently used for encapsulation of anticancer drug molecules. MIL-100(Fe) and MIL-53(Fe) showed high storage performance for busulfan (0.25 g/g, and 0.14 g/g, respectively).[17] The reported busulfan uptakes in these MOFs are higher than traditional drug carriers such as liposomes or polymeric nanoparticles which have almost 0.05-0.06 g/g uptake.[17] Anand et al.[18] used MIL-100(Fe) for the controlled delivery of doxorubicin and the drug loading was reported as 0.09 g/g. Storage of the antitumor agent 5-fluorouracil (5-FU) was also investigated in Zn and Cu-based MOFs. Sun et al.[19] showed that ZIF-8 (zeolitic imidazolate framework) has a high 5-FU loading (0.45 g/g). They later showed that a Zn-MOF can outperform ZIF-8 in terms of 5-FU uptake (0.5 g/g).[20] The highest 5-FU uptake (0.82 g/g) was achieved using one of the most commonly studied MOFs in the literature, CuBTC.[21] Lin et al.[22] performed the first study in the literature showing that MOFs can be efficient oral anticancer drug carriers. They showed that a low cytotoxic porphyrin-based MOF, PCN-221 (PCN refers to a porous coordination network) can be an oral drug carrier for anticancer drug, methotrexate (MTX). The loading of MTX in PCN-221 was reported to be 0.4 g/g. The same group later synthesized two zinc-based porous MOFs, namely ZJU-64 and ZJU-64-CH_3, and reported moderate MTX loadings, 0.13 g/g and 0.11 g/g, respectively, for these two MOFs.[23] Rojas et al.[24] examined concurrent adsorption and diffusion of an anticancer drug, RAPTA-C and a bioactive gas, nitric oxide (NO) in CPO-27-Ni. McKinlay and co-workers[25] showed that CPO-27-Ni, CPO-27-Co and CuBTC can deliver an antibiotic drug molecule, the metronidazole and NO simultaneously at different rates.

All these initial experiments showed that MOFs are highly promising materials for storage of anticancer drugs and encapsulation of two different anticancer drug molecules into MOFs is possible. Considering the very high number of available MOFs in the literature, it is not possible to test every single MOF for the storage and delivery of drug molecules using purely experimental techniques. Highly accurate computational methods are required to predict the drug storage and delivery performances of MOFs prior to extensive experimental efforts in order to identify the most promising materials. However, the number of computational studies that investigate MOFs for drug storage and delivery is very limited in the literature due to the challenge of modeling confinement of large drug molecules in MOFs at the molecular-level, which requires significant computation time due to the long

equilibration process. Molecular simulations were used to examine storage and delivery of ibuprofen in MIL-101(Cr) and UMCM-1.[26] The predicted ibuprofen loading in UMCM-1 (1.36 g/g) was higher than the one in MIL-101(Cr) (1.11 g/g) due to highly porous structure of UMCM-1 (2.28 cm^3/g) compared to MIL-101(Cr) (1.96 cm^3/g). Bei and co-workers[27] performed molecular simulations to determine ibuprofen uptake in bio-MOF-1, bio-MOF-11, bio-MOF-100, UMCM-1 and showed slow drug diffusion in these MOFs. Bernini et al.[28] examined different biocompatible MOFs such as CD-MOF-1(CD:cyclodextrin), bio-MOF-100 and MOF-74 and predicted their ibuprofen uptakes. Bueno-Perez et al.[29] investigated storage of ibuprofen in HMOF-1(heterometal organic framework), MIL-47(V) and MIL-53(Cr) in the liquid medium and showed that water does not affect the saturation drug uptake of MOFs. We recently performed molecular simulations for a larger number of MOFs to examine adsorption and diffusion of ibuprofen and two cosmetic molecules, caffeine and urea, in 24 different bio-compatible MOFs.[30] Our results showed that bio-MOF-100 and MOF-74 materials outperform traditional drug storage materials such as zeolite and mesoporous silica for storage of these three molecules. Kotzabasaki et al.[31] recently performed molecular simulations to predict the uptake of an anticancer drug, gemcitabine in IRMOF-74-III and its OH functionalized counterpart. The saturated drug loading for both MOFs was found to be the same (1.13 g/g), outperforming lipid-coated mesoporous silica nanoparticles (0.4 g/g). They also showed that pore volume has more influence on the drug uptake of a MOF rather than the functionalization of the framework, consistent with the results of our previous work.[30]

This literature review shows that there is still no experimental and/or computational study which examines the potential of MOFs for concurrent adsorption and diffusion of two anticancer drug molecules. In this work, we performed molecular simulations to investigate storage and delivery of two anticancer drugs in a series of MOF materials. Considering biocompatibility of both the metal and bridging ligand of MOFs is important. Several MOFs have toxic metals (Co, Cd, etc.) in their structures that limit their biological usage. The MOFs we considered in this study, MOF-74 materials, are biocompatible due to the low toxicity of Mg and Zn metals and carboxylic linker under physiological conditions. Mg^{2+} is the one of the most abundant cation in the human body and bond tissues contain both Mg[32] and Zn.[7] We focused on MTX and 5-FU as the anticancer drug molecules because recent studies showed that simultaneous administration of MTX and 5-FU increases the therapeutic efficacy of these drugs in treatment of colorectal cancer, which is one of the most common cancers that causes

a high rate of morbidity based on the global cancer statistics.[33] We performed configurational bias Monte Carlo (CBMC) and molecular dynamics (MD) simulations to compute adsorption and diffusion of MTX and 5-FU molecules in MOFs. Results of our molecular simulations were first compared with the available experimental uptake data of various MOFs. Motivated from the good agreement between our computational predictions and experiments, we computed saturated MTX and 5-FU loadings of MOF-74 materials. We then selected the top performing materials for drug storage and computed both single-component and binary adsorption isotherms of MTX and 5-FU molecules in MOFs to examine the drug adsorption mechanism in detail. We finally performed MD simulations to investigate diffusion of molecules through the pores of MOFs considering both the single-component drugs and their binary mixtures for the first time in the literature.

2. Computational Details

In order to validate our computational methodology, we first compared our predictions with the available experimental data for MTX and 5-FU uptake in several MOFs, such as PCN-221,[22] ZJU-64-CH_3,[23] Zn-MOF (GDMU),[34] Cu-MOF (GDMU-2),[35] ZIF-8[36] and CuBTC.[37] PCN-221 has Zr ions linked by porphyrin derivative ligands, having cages of 11×20 Å in size.[22] ZJU-64-CH_3 has Zn ions linked by adenine and carboxylate-based ligands, showing a three dimensional framework with one dimensional channels (16×19 Å).[23] GDMU and GDMU-2 are polyhedral MOFs which have cages with large voids and open-channel-type pores.[34, 35] GDMU has cages with 9×12 Å whereas GDMU-2 has cages of 4×15 Å. Among these MOFs, ZIF-8 and CuBTC are the two widely studied MOFs in the literature. ZIF-8 is a prototypical ZIF structure that has Zn metal ions linked by 2-methylimidazolate ligands, showing a three dimensional framework with pore sizes of 3.4×11.5 Å. CuBTC has open Cu sites linked by benzene-1,3,5-tricarboxylate which results in a three dimensional framework with large pore sizes of 9×5 Å.

In our previous work,[30] we showed that MOF-74 materials are promising for storage and delivery of ibuprofen, caffeine and urea due to their large pore volumes. Therefore, we considered the same family as host materials for storage of anticancer drug molecules in this work. We investigated 10 MOFs from MOF-74 series in order to have a representative material set having different structural properties such as pore sizes, porosities, surface areas. The Cambridge Crystallographic Data Center (CCDC)[38] reference code of MOF-74 is VOGTIV and it has Mg as the metal and dioxidoterephthalate (DOT) as the organic linker. 9 different isoreticular structures of MOF-74 exist, namely RAVXIX, RAVXET, RAVWUI,

RAVXAP, RAVWIW, RAVWOC, RAVWES, RAVWAO, and RAVVUH. All MOF-74 materials have Mg except RAVWUI which has Zn as the metal. Crystal structures of these MOFs were taken from the CCDC.[38] Solvent molecules, if present, were removed before molecular simulations. Stability of the MOFs after the solvent removal was confirmed from the corresponding experimental studies.[39] These MOFs all have permanent porosities and high thermal stabilities up to 300°C.[39] Structural properties of MOFs such as pore volumes, pore limiting diameters (PLD), largest cavity diameters (LCD) and accessible surface areas were calculated using Zeo^{++} software[40] and all these properties were listed in Table 1. Surface area calculations were performed using a probe radius of 1.86 Å. For pore volume calculations, probe radius was set to zero. As shown in Table 1, MOF-74 has the lowest pore volume (0.7 cm^3/g) and the smallest surface area (1621 m^2/g). As the number of phenylene rings increases from one (MOF-74) to ten (RAVXIX) as shown in Figure 1, pore volumes, surface areas and pore sizes of MOFs increase.

We initially performed configurational bias-Monte Carlo (CBMC) simulations using the fixed pressure task in sorption module of Materials Studio 8.0[41] to determine the adsorbed number of MTX and 5-FU molecules in MOFs at 1 bar and 37 °C. Structures of MTX and 5-FU were taken from PubChem.[42] DMol3 was used to optimize the geometry of drug molecules and ESP (ElectroStatic Potential) charges were assigned to all atoms in the molecules. For DMol3 calculations, generalized gradient approximation, the Perdew-Wang-91 (GGA-PW91) functional was used and the double numerical plus polarization (dnp) with a basis file of 3.5 was implemented.[41] Torsion degrees of freedom for MTX molecule were defined prior to the CBMC simulations. The interactions of drug molecules with the MOFs were modeled using Lennard-Jones (LJ) 12-6 and Coulomb potentials. LJ parameters were taken from the Universal Force Field (UFF)[43] both for MOFs and drug molecules. For the van der Waals terms, atom-based summation method was used with the cubic spline truncation. 15.5 Å was used as a cut-off radius for van der Waals terms. Ewald summation method with 10^{-4} kcal/mol accuracy was used to calculate electrostatic interactions. The atomic charges of MOFs were estimated using the EQeq (Extended Charge Equilibration) method.[44] A 2×2×2 supercell was created for MOF-74, RAVVUH and RAVWAO whereas 1×1×1 unit cell was used for the other MOFs. Simulations were performed with trial configurations consist of 10^6 cycles for the equilibration and 10^6 cycles for the production step. More detailed information about the CBMC simulations can be found in our previous work.[30]

Performing molecular simulations for single-component and mixture drug adsorption in MOFs at a wide pressure range is computationally demanding therefore, we selected the most promising four MOFs which exhibit high drug uptake at 1 bar and 37 °C. We then computed single-component and binary adsorption isotherms of MTX and 5-FU in these four MOFs at a wide range of fugacity (10^{-16}-1 bar) at 37 °C. Sorption module in Materials Studio reports the drug loadings as a function of the reservoir fugacity. In order to analyze adsorption strength of drugs in MOFs, isosteric heat of adsorption (Q_{st}) was calculated. Q_{st} shows the average binding energy of an adsorbed molecule and can be calculated from the ensemble average fluctuations as follows,[45]

$$Q_{st} = RT - \left(\frac{\langle U_{ads} \times N_{ads} \rangle - \langle U_{ads} \rangle \times \langle N_{ads} \rangle}{\langle N_{ads}^2 \rangle - \langle N_{ads} \rangle \times \langle N_{ads} \rangle} \right) \quad (1)$$

where T is the temperature, R is ideal gas constant, $\langle U_{ads} \rangle$ is the average potential energy of adsorbed phased and $\langle N_{ads} \rangle$ is the average number of molecules in the simulation system.

We then performed MD simulations for the two most promising MOFs to examine drug diffusion. Diffusion of both single-component and binary mixtures of MTX and 5-FU molecules was studied using the forcite module of Materials Studio.[41] In MD simulations, the initial configurations were taken from the CBMC simulations computed at 10^{-7} bar and 37 °C. UFF was used for bond stretching, angle bending and dihedral torsions as implemented in Materials Studio. Geometry optimization steps were initially performed for structures until the following convergence criteria were reached: 10^{-4} kcal/mol for energy, 5×10^{-3} kcal/mol Å for forces and 5×10^{-5} Å for displacement. The cell geometry was not allowed to change during the optimization step. After optimization, MD simulations within the NVT ensemble were performed with a step size of 1 fs up to a total of 7 ns at 37 °C. Nose-Hoover-Langevin (NHL) thermostat[45] was used to keep the temperature constant. The mean square displacement (MSD) of drug molecules was computed as follows where N is the number of drug molecules and $r_j(t)$ is the position of the j^{th} drug molecule at time t:

$$MSD(t) = \frac{1}{N} \sum_{j=1}^{N} \left\langle \left[\vec{r}_j(t) - \vec{r}_j(0) \right]^2 \right\rangle \quad (2)$$

In our recent study,[30] we performed MD simulations considering both rigid and flexible structures of several MOFs, including bio-MOF-100, bio-MOF-102 and RAVXIX to examine ibuprofen diffusion. Our results showed that when the flexibility of MOFs was considered in

molecular simulations, ibuprofen diffusion slightly increased but it was still very slow to surpass the cell boundaries of the MOFs. Based on this previous result, we performed MD simulations using rigid frameworks in this work to save significant computational time.

3. Results and Discussions

We first compared our predictions with the available experimental data for MTX and 5-FU uptake in six different MOFs, PCN-221, ZJU-64-CH_3, GDMU, GDMU-2, ZIF-8 and CuBTC. We performed the CBMC simulations at 37 °C and 1 bar to compute the maximum MTX and 5-FU uptake in MOFs. Only for ZJU-64-CH_3, we performed our molecular simulations at 60 °C and 1 bar to be consistent with the experimental study.[23] Figure 2 shows comparisons of simulated uptakes and experimentally measured uptakes of MTX and 5-FU in MOFs. Drug uptake capacities were reported as weight percents (wt%) to be consistent with the literature. As shown in Figure 2, our molecular simulations are in a good agreement with the experimentally reported data. Only for CuBTC, molecular simulations slightly underpredicted 5-FU uptake. This may be attributed to the crystal structure of CuBTC. In the experimental study,[37] commercial structure of CuBTC, Basolite^{TM} C300, was used. CuBTC has more than forty different crystal structures in the CCDC[46] with different surface areas and pore volumes as a result of different synthesis and activation methods. It is not known which CCDC structure is exactly the same with the commercial CuBTC and we chose the first reported structure, FIQCEN, from CCDC to perform molecular simulations. The crystal structure of CuBTC that we used in our simulations may have different structural properties than the one examined in the experiments, which can be the reason of discrepancy between simulations and experiments.

After validating our computational methodology, we computed saturated MTX and 5-FU uptakes of ten MOF-74 materials which have not been experimentally studied for MTX and 5-FU storage to date. Figure 3(a) shows predicted MTX uptake capacities of MOF-74 materials at 1 bar, 37 °C. The dashed line shows the available experimental data of the MOF which has the maximum MTX uptake in the literature, PCN-221. As shown in Figure 3(a), all MOFs except MOF-74 (VOGTIV) can exceed the MTX uptake of PCN-221. RAVXIX has the maximum MTX uptake (2.78 g/g). This capacity is much higher than those of other materials reported in the literature such as mesoporous silica materials, SBA-15 (0.11 g/g),[47] SBA-16 (0.14 g/g),[47] mesoporous silica molecular sieves MCM-41 (0.08 g /g)[47], PLGA-based micelles (0.31 g/g)[48] and magnetic nanocomposites such as Fe_3O_4@LDH (0.18 g/g).[49] The high drug uptake of RAVXIX can be attributed to its extremely high pore volume (3.7 cm^3/g)

and large pore sizes (53.3×53.6 Å) compared to traditional porous materials. Similarly, we computed 5-FU uptake in MOF-74 materials and results were shown in Figure 3(b). The dashed line represents the 5-FU uptake of CuBTC, which was experimentally reported to have the highest 5-FU uptake. All MOF-74 materials except VOGTIV can outperform CuBTC for 5-FU uptake as shown in Figure 3(b). The maximum 5-FU uptake was found as 4.24 g/g for RAVXIX. Comparison with other traditional 5-FU storage materials demonstrates that MOF-74 materials outperform zeolite ZSM-5 (0.38 g/g)[50] and polymeric materials such as cross-linked microspheres (0.15 g/g).[51] All these results suggest that due to their highly porous structures, MOF-74 materials are highly promising candidates for storage of anticancer drug molecules MTX and 5-FU.

We also investigated relations between the structural properties of MOFs and their drug uptakes. Establishing this type of relations is important to guide the experimental synthesis of new MOFs with exceptionally high storage capacities for target drug molecules. Figure 4 shows the linear correlations between the predicted MTX and 5-FU uptakes of MOFs and their calculated pore volumes, PLDs and LCDs. Both MTX and 5-FU uptakes increase as the pore volumes and pore sizes of MOFs increase. This result is in agreement with our previous study[30] where correlations between ibuprofen uptake of MOFs and their structural properties were examined. As shown in Figure 4, MOF-74 has the lowest MTX (0.31 g/g) and 5-FU (0.71 g/g) uptake due to its low pore volume (0.7 cm^3/g) and small pore sizes (10.76×11.64 Å). RAVVUH and RAVWAO have similar MTX uptakes (~0.7 g/g) but RAVWAO (1.31 g/g) has slightly higher 5-FU uptake than RAVVUH (1.2 g/g). This can be attributed to the higher pore volume of RAVWAO (1.42 cm^3/g) compared to RAVVUH (1.23 cm^3/g) because they have similar pore apertures (~17 Å). As the pore volume increases from 1.81 cm^3/g (RAVWES) to 2.28 cm^3/g (RAVWIW), MTX uptake increases from 1.36 to 1.52 g/g and 5-FU uptake increases from 2.05 to 2.45 g/g. RAVXET and RAVWUI have similar pore volumes (~2.5 cm^3/g) but their pore sizes are different. The larger pore apertures of RAVXET lead to higher MTX uptake as expected. RAVXIX has the highest MTX (2.78 g/g) and 5-FU (4.24 g/g) uptakes because it has the highest pore volume (3.74 cm^3/g) and the largest pore size (53.26×53.58 Å) among the ten MOFs we considered. Correlations shown in Figure 4 indicate that structural properties of MOFs, pore sizes and available pore volumes strongly affect drug uptake performances of materials. In fact, these results suggest that desired drug loadings can be achieved via pore expansion strategy which is commonly used in the

synthesis of isoreticular MOFs, materials having the same topology and metal site but different organic linkers at varying length.

In order to understand the drug adsorption mechanism in MOFs, we selected the top four MOFs with the highest drug loadings and computed both the single-component and equimolar mixture adsorption isotherms of MTX and 5-FU in these MOFs. Figure 5 shows adsorption isotherms of MTX and 5FU in RAVXIX, RAVXAP, RAVXET and RAVWUI. Adsorption isotherms can be broadly divided into three pressure regions. At very low pressures, 10^{-16}-10^{-10} bar, adsorption isotherms of drug molecules in MOFs are similar to each other and they approach to zero in the infinite dilution limit as expected. At 10^{-10}-10^{-5} bar, MTX molecules are more strongly adsorbed than 5-FU molecules in all MOFs except RAVXAP. Since MTX molecule ($C_{20}H_{22}N_8O_5$) has higher number of atoms than 5-FU molecule ($C_4H_3FN_2O_2$), it has more interaction sites with the MOF atoms for adsorption. As a result of energetic effects, MTX molecules are strongly confined in the pores of MOFs compared to 5-FU molecules. At 10^{-5}-1 bar, adsorption favors 5-FU. The average Q_{st} values at this fugacity region for MTX (60-75 kcal/mol) are higher than the ones calculated for 5-FU (24-29 kcal/mol) in MOFs. However, entropic effects dominate the energetic effects and as the fugacity increases, small 5-FU molecules (~5.4×5.0 Å) can find space and fill the pores whereas large MTX molecules cannot be adsorbed into the MOFs' pores. The trends in single-component adsorption isotherms of drug molecules can be discussed in terms of the calculated Q_{st} values shown in Figure S1. The positive values of Q_{st} indicate that MTX and 5-FU adsorption in RAVXIX, RAVXAP, RAVXET and RAVWUI is endothermic in nature. The average Q_{st} values for MTX (55-69 kcal/mol) are higher than the ones calculated for 5-FU (22-31 kcal/mol) in MOFs at a pressure range of 10^{-16}-1 bar, supporting stronger adsorption of MTX compared to the 5-FU adsorption. Figures S1(a-b) show that Q_{st} values are almost constant with slight increase as the fugacity increases, which can be attributed to the attractive interactions between the adsorbed MTX molecules in the MOFs' pores.

Single-component drug adsorption can be very different than the mixture drug adsorption. Two different drug molecules may be competing for the same adsorption site of the MOF which may result in decreased drug uptakes in the mixture case compared to the single-component case. Therefore, we also compared the single-component adsorption isotherms of drug molecules with their mixture adsorption isotherms in Figure 5. As shown in Figure 5, both MTX and 5-FU uptakes decrease in the mixture adsorption compared to the

single-component case. The decrease is more pronounced for the strongly adsorbed molecule, MTX. The average value of Q_{st} obtained from the mixture simulations of MTX (48-63 kcal/mol) are lower than the ones obtained from single-component MTX adsorption simulations (55-69 kcal/mol) at a pressure range of 10^{-16}-1 bar. For 5-FU, the average Q_{st} values computed from the mixture adsorption (26-31 kcal/mol) are in the same range with the ones calculated from the single-component 5-FU adsorption simulation (22-31 kcal/mol). These findings also confirm the strong decrease in MTX loadings and slight decrease in 5-FU loadings in mixture adsorption. As a result, the total of mixture drug uptakes is lower than the total of single-component uptakes at 1 bar. For example, the total of single-component MTX and 5-FU uptakes are 4.42, 4.78, 5.42 and 7.02 g/g whereas the total of mixture uptakes are 2.48, 2.70, 2.99 and 3.99 g/g in RAVXET, RAVWUI, RAVXAP and RAVXIX, respectively.

In order to develop an efficient drug delivery system, not only high drug storage but also slow drug release is desired. We investigated MTX and 5-FU diffusion in the two MOFs, RAVXIX and RAVXAP, which were identified as the top two promising materials for MTX and 5-FU storage. Figure 6 shows both the single-component and mixture diffusion of MTX and 5-FU in these MOFs. The number of molecules considered in MD simulations was taken from the CBMC simulations. Assessing diffusion of large drug molecules in large-pored MOFs is highly computationally demanding. Therefore, a low pressure, 10^{-7} bar, was chosen to observe the diffusion of MTX and 5-FU in a reasonable computation time. As shown in Figure 6, both MTX and 5-FU molecules cannot pass the cell boundaries of MOFs because diffusion of these two drug molecules in MOFs is very slow as desired in the controlled drug delivery systems to eliminate the burst effect of rapid drug release within a short period of time. Figure 6(a) shows that single-component 5-FU diffusion is faster than that of MTX in RAVXIX. This is expected because small 5-FU molecules can diffuse faster through the large pores of RAVXIX compared to heavy and bulky MTX molecules. When the binary drug diffusion is considered, diffusion of MTX molecules slightly increases whereas diffusion of 5-FU molecules does not significantly change. This result can be discussed considering the number of adsorbed drug molecules available in the pores, which is given in Table 2. The number of slowly diffusing MTX molecules decreases from 23 to 5 in one unit cell of MOF when a drug mixture is considered. Instead of having 23 MTX molecules, 5 MTX and 6 5-FU molecules exist in the pores of RAVXIX in the mixture case. As a result, steric hindrance effects decrease and the fast diffusing 5-FU molecules in the mixture accelerate the diffusion of MTX molecules. Diffusion trends of drug molecules can be also discussed in terms of

different affinity of RAVXIX for MTX and 5-FU. Q_{st} data for adsorption of single-component drug molecules and drug mixtures are given in Table 3. The Q_{st} value for MTX decreases from 57.4 to 52.6 kcal/mol when the adsorption of a drug mixture is considered. This decrease suggests that adsorption affinity of RAVXIX for MTX decreases and as a result diffusion of MTX molecules increase. On the other hand, Q_{st} for 5-FU molecules is computed to be almost the same, ~21 kcal/mol, in both single-component and binary drug adsorption cases. Therefore, diffusion rates of 5-FU molecules do not change when an equimolar mixture of MTX and 5-FU is considered in the MOF. At that point, it is important to note that the differences between Q_{st} values of the same drug molecules in two different MOFs can be explained by the different adsorption affinities of two frameworks due to their ligand chemistries and structural properties as we discussed in Figure 4.

Figure 6(b) shows both the single-component and mixture diffusion of MTX and 5-FU in RAVXAP. Similar to RAVXIX, single component 5-FU diffusion is much faster than single-component MTX diffusion in RAVXAP. Compared to the single-component case, diffusion of MTX molecules slightly increases whereas diffusion of 5-FU molecules decreases in the mixture case. The fast diffusing 5-FU molecules in the mixture accelerate the diffusion of slowly diffusing MTX molecules. On the other hand, increased number of MTX molecules in the mixture (7 MTX molecules in single-component case, 10 MTX molecules in the mixture case) slow down the diffusion of 5-FU molecules. We can also discuss the diffusion trends considering Q_{st} values. Table 3 shows that Q_{st} value for MTX decreases from 53.1 to 52 kcal/mol in the binary adsorption case, explaining the slight increase in MTX diffusion. On the other hand, Q_{st} value for 5-FU molecules increases from 29.4 to 32.2 kcal/mol. The higher affinity of RAVXAP for 5-FU results in a decrease in diffusion of 5-FU molecules. Overall, MD simulations showed that diffusion of both single-component drugs and their mixtures is very slow in RAVXIX and RAVXAP, suggesting that these MOFs can have a great potential in controlled-drug delivery systems.

It is also important to understand the interactions between drug molecules and MOFs. Although MOF-74 materials have very large pores, due to the strong interactions between the framework and drug molecules, diffusion of drugs is very slow within the pores of these materials. MD snapshots for the equilibrium configurations of MTX and 5-FU in RAVXIX and RAVXAP shown in Figures S2-S3 demonstrate that the metal cations are the favorable adsorption sites for the drug molecules. We also performed energy analysis both for single-

component drugs and their mixtures during MD simulations and results were shown in Figures S4-S5. As can be seen from these figures, the non-bonded energy (electrostatic and van der Waals) for MTX and 5-FU diffusion in RAVXIX was dominated by the electrostatic interactions. For example, average electrostatic energy during MTX diffusion in RAVXIX was computed as -9965 kcal/mol whereas the dispersion energy was computed as 161 kcal/mol. Similarly, van der Waals energy (-63.01 kcal/mol) during 5-FU diffusion in RAVXIX was calculated to be much lower than the electrostatic energy (-1553.68 kcal/mol). These results indicate that both drug molecules have strong electrostatic interactions with the atoms of RAVXIX. This result is consistent with the study of Bernini et al.[28] who reported that metal sites of MOF-74 are responsible for strong ibuprofen adsorption and slow ibuprofen diffusion. In our previous work,[30] we reported strong adsorption of ibuprofen (30 kcal/mol) and its slow diffusion in RAVXIX. In this work, adsorption of MTX in RAVXIX (60 kcal/mol) was found to be much stronger than the adsorption of ibuprofen in RAVXIX and adsorption of 5-FU (22 kcal/mol and 30 kcal/mol, respectively) was also found to be close to the adsorption of ibuprofen in RAVXIX. Therefore, this MOF is highly promising not only due to its high drug storage capacity but also its slow drug delivery.

We aimed to provide molecular-level insight into the drug adsorption and diffusion mechanisms of MOFs using molecular simulations. Although thousands of MOF structures have been reported,[38] only a small number of MOFs has been investigated for drug storage and delivery applications. We considered an equimolar mixture of MTX and 5-FU molecules in this study. The maximum tolerated doses of each anticancer drug should be determined for their concurrent administration. The knowledge on pharmacokinetics and convenient biodistribution of drug molecules is also required. These issues are more likely to be addressed by further experimental studies once the most promising MOFs for drug storage and delivery are identified by the computational studies. As we reviewed in the introduction, studies showing that MOFs can be efficient oral anticancer drug carriers recently appeared in the literature. Therefore, the results we demonstrated in this work will be highly useful to understand the drug-MOF interactions which can guide the practical applications of MOFs as drug carrier system.

4. Conclusion

In this study, we examined the potential of ten different MOF-74 materials as binary drug carrier systems. Understanding simultaneous adsorption and diffusion of anticancer drug molecules in the host material is important to develop combination therapy for cancer

treatment. We performed CBMC and MD simulations to compute storage and diffusion of two anticancer drugs, MTX and 5-FU, in MOFs. RAVXIX was identified as the top performing MOF which has the highest MTX (2.8 g/g) and 5-FU (4.2 g/g) uptakes due to its extremely large pore volume. We showed strong linear relations between pore volumes/pore sizes and drug uptake capacities of MOFs. Both single-component and binary adsorption isotherms of MTX and 5-FU molecules were computed in four MOF-74 materials. Results showed that RAVXET, RAVWUI, RAVXAP and RAVXIX can be potential materials for storage of MTX and 5-FU mixtures. We also examined single-component and mixture diffusion of MTX and 5-FU molecules through the pores of MOFs using MD simulations. Slow diffusion of drug molecules in MOF-74 materials suggested that MOFs have strong potential as multi-drug carrier systems for combination therapies in cancer research. The computational methodology that we provided in this work will be useful to effectively identify the most promising MOFs for target drug storage and delivery applications prior to extensive experiments. By providing fundamental insights at the molecular-level on the drug adsorption and diffusion mechanism of MOFs, this study will also guide the design and development of new MOFs as multi-drug delivery systems.

Acknowledgements: This project is supported by Koç University Seed Fund Program (Grant no. SF.00057).

View Article Online
DOI: 10.1039/C7TB01764B

Graphical Abstract

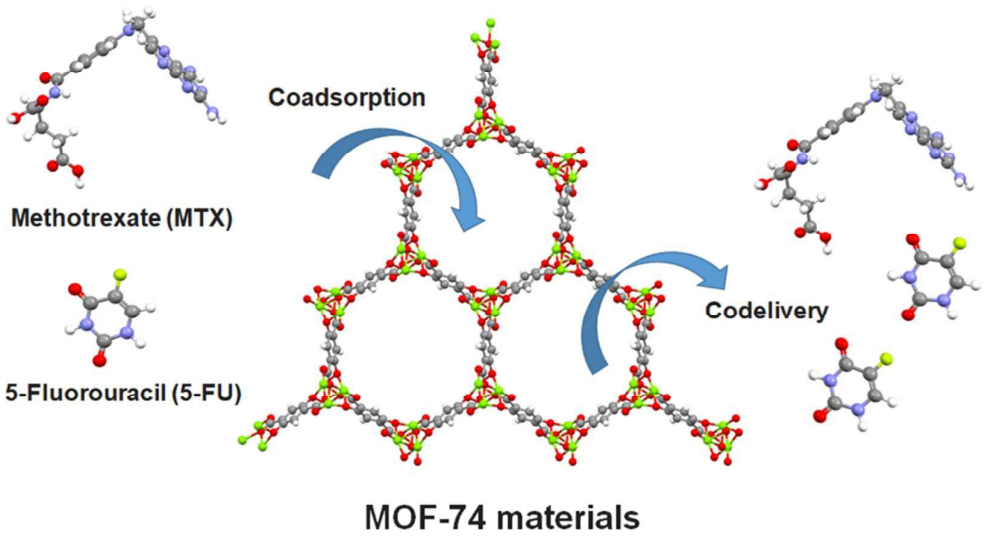

View Article Online
DOI: 10.1039/C7TB01764B

Table 1. Structural properties of MOF-74 materials

MOF	Pore volume (cm^3/g)	Surface area (m^2/g)	PLD (Å)	LCD (Å)
VOGTIV (MOF-74)	0.70	1621	10.76	11.64
RAVVUH	1.23	2228	16.38	17.18
RAVWAO	1.42	2621	17.51	17.93
RAVWES	1.81	2759	23.63	24.44
RAVWIW	2.28	3018	30.14	30.70
RAVWOC	2.11	2916	27.56	28.22
RAVWUI	2.55	2893	36.43	36.79
RAVXAP	2.96	3360	34.36	34.86
RAVXET	2.54	2809	38.07	38.23
RAVXIX	3.74	3036	53.26	53.58

Table 2. The number of molecules per unit cell of MOF considered in MD simulations at 10^{-7} bar and 37 °C. In parenthesis, corresponding drug loading (g/g) was given.

Conditions	RAVXIX	RAVXAP
Single-component MTX	23 (1.00)	7 (0.38)
Single-component 5-FU	14 (0.17)	20 (0.35)
MTX in MTX/5-FU mixture	5 (0.20)	10 (0.51)
5-FU in MTX/5-FU mixture	6 (0.07)	18 (0.27)

Table 3. The isosteric heat of adsorption values (kcal/mol) for MTX and 5-FU uptake at 10^{-7} bar and 37 °C

Conditions	RAVXIX	RAVXAP
Single component MTX	57.40	53.09
Single component 5-FU	21.46	29.42
MTX in MTX/5-FU mixture	52.65	51.99
5-FU in MTX/5-FU mixture	21.52	32.22

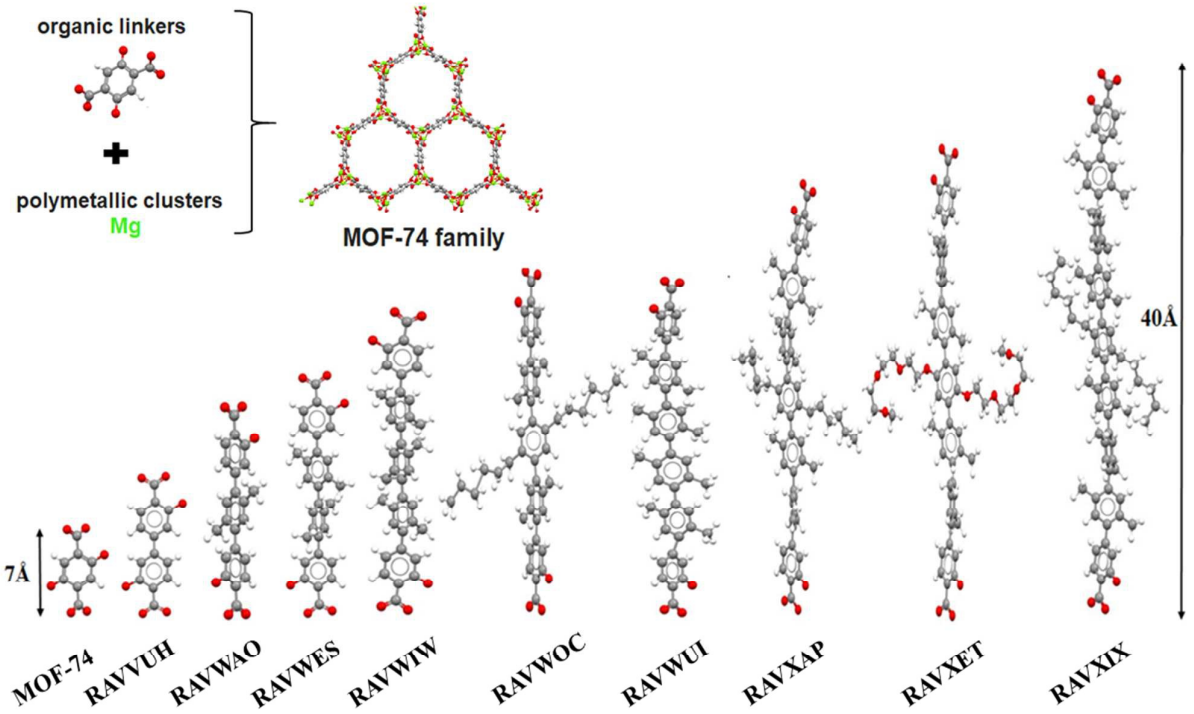

Figure 1. Expansion of the organic linker of MOF-74 structures.

View Article Online
DOI: 10.1039/C7TB01764B

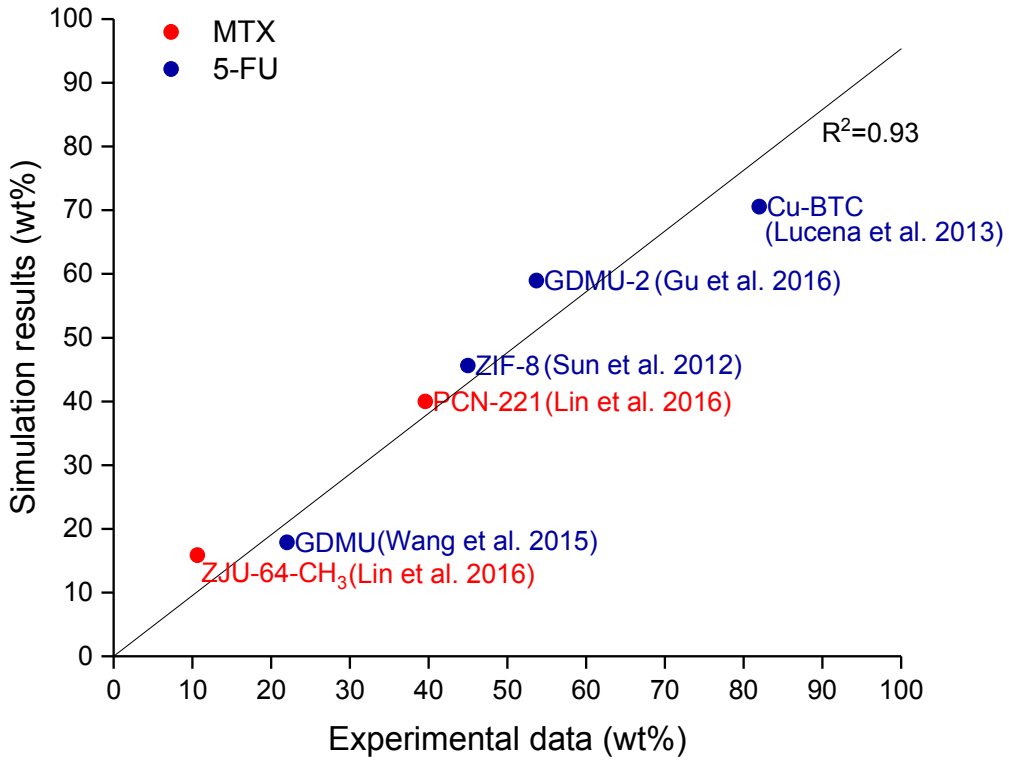

Figure 2. Comparison of our simulated drug uptakes of MOFs with the experiments.[22, 23, 34-37] Red (blue) points represent MTX (5-FU) uptake.

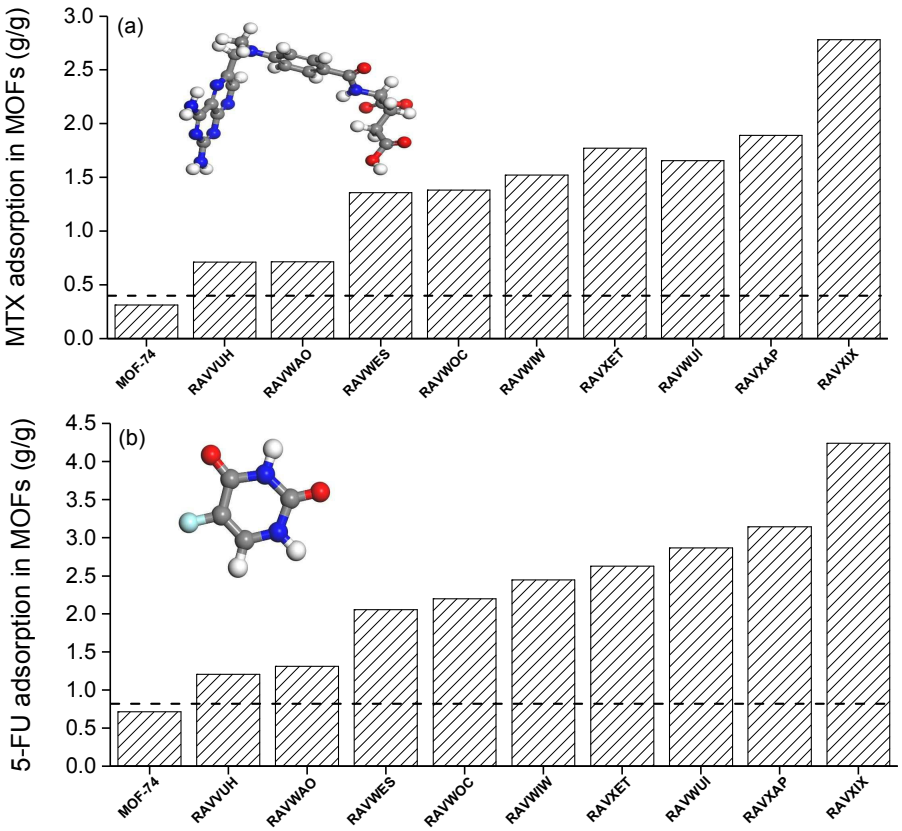

Figure 3. (a)MTX (b)5-FU adsorption in MOF-74 materials (g drug/g MOF). The dashed lines in (a) and (b) show the current upper limit for experimental MTX and 5-FU uptake in PCN-221 and CuBTC, respectively.

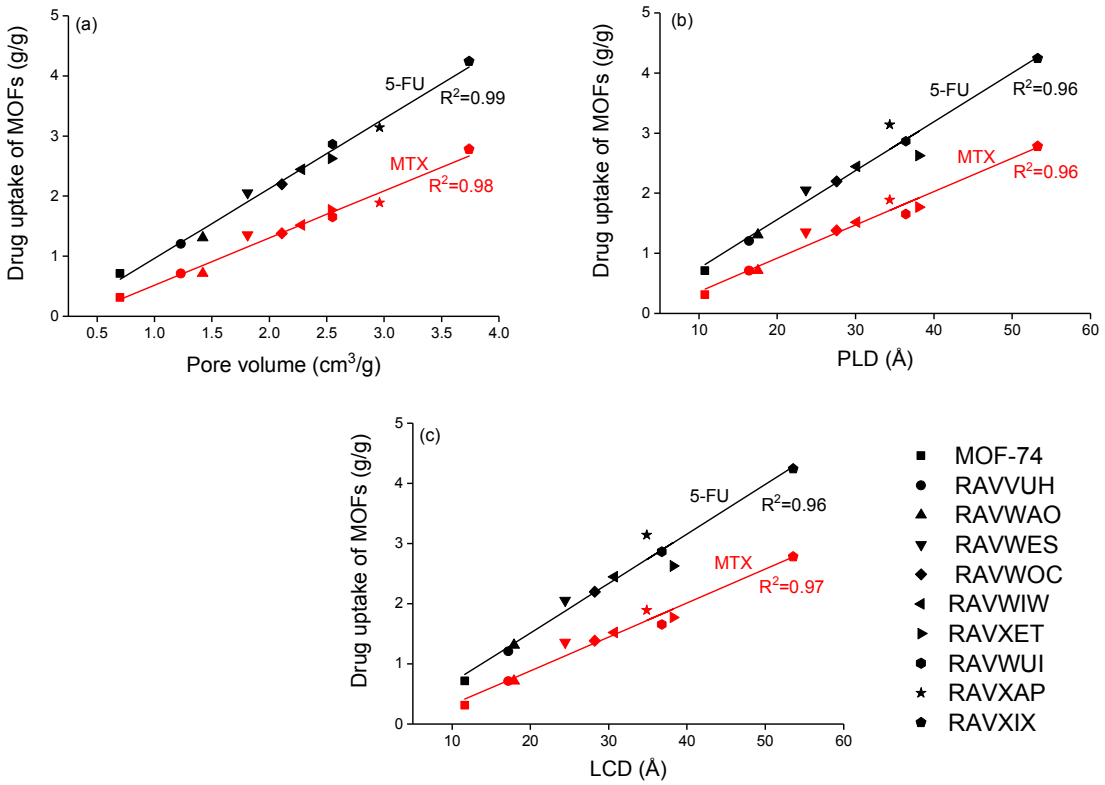

Figure 4. Correlations between drug uptakes of MOFs and their (a)pore volumes, (b)PLDs, and (c)LCDs.

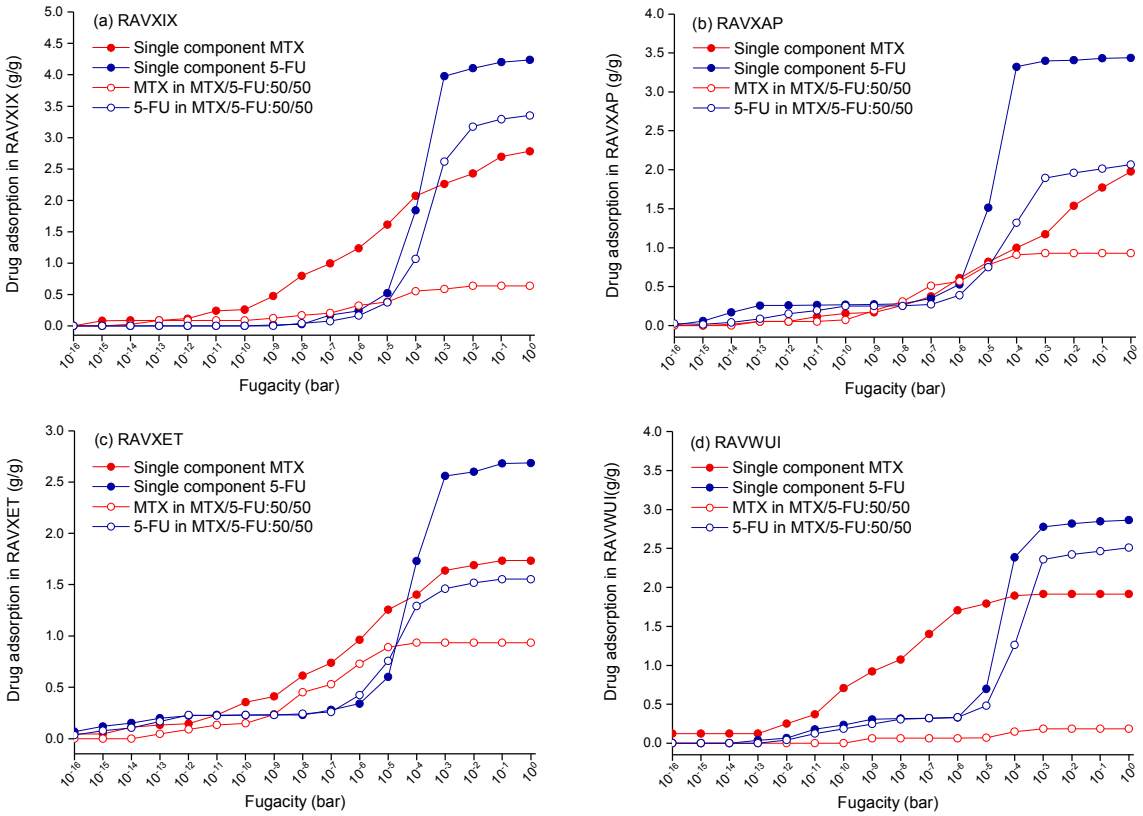

Figure 5. Single-component and mixture adsorption isotherms of MTX and 5-FU in (a)RAVXIX, (b)RAVXAP, (c)RAVXET and (d)RAVWUI.

View Article Online
DOI: 10.1039/C7TB01764B

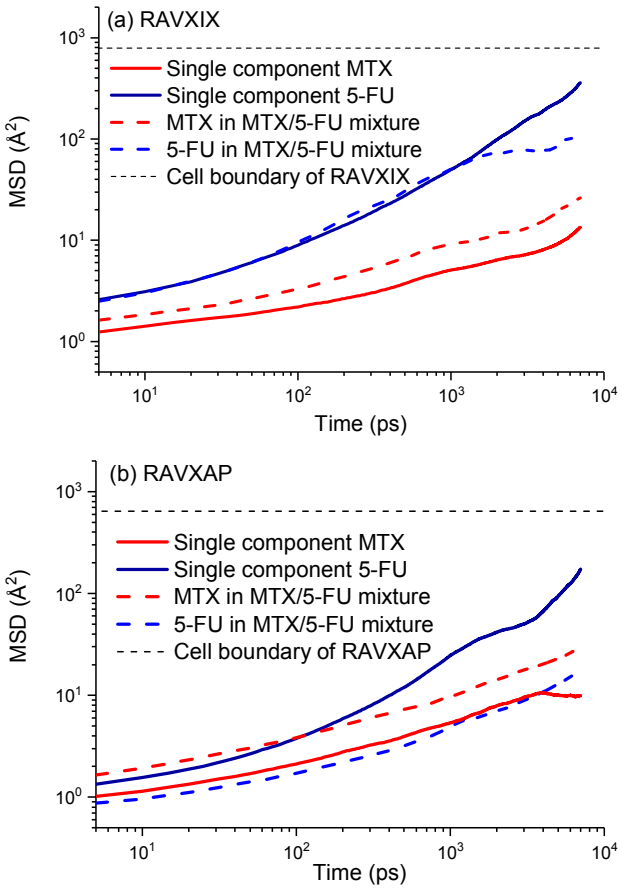

Figure 6. Single-component and mixture diffusion of MTX and 5-FU in (a)RAVXIX and (b)RAVXAP.

References:

1 R. Thipparaboina, R. B. Chavan, D. Kumar, S. Modugula and N. R. Shastri, *Colloids Surf., B*, 2015, **135**, 291-308.
2 Q. Hu, W. Sun, C. Wang and Z. Gu, *Adv. Drug Delivery Rev.*, 2016, **98**, 19-34.
3 N. Ashwanikumar, N. A. Kumar, S. A. Nair and G. S. V. Kumar, *Colloids Surf., B*, 2014, **122**, 520-528.
4 Y.-M. Ning, K. He, R. Dagher, R. Sridhara, A. T. Farrell, R. Justice and R. Pazdur, *Oncol. (Williston Park, NY)*, 2007, **21**, 1503-1508.
5 T.-H. Kim, G. J. Lee, J.-H. Kang, H.-J. Kim, T.-i. Kim and J.-M. Oh, *BioMed Res. Int.*, 2014, **2014**, 1-11.
6 F. Tang, L. Li and D. Chen, *Adv. Mater.*, 2012, **24**, 1504-1534.
7 S. Keskin and S. Kızılel, *Ind. Eng. Chem. Res.*, 2011, **50**, 1799-1812.
8 Q. Zhao, C. Huang and F. Li, *Chem. Soc. Rev.*, 2011, **40**, 2508-2524.
9 J.-B. Liu, C. Yang, C.-N. Ko, K. Vellaisamy, B. Yang, M.-Y. Lee, C.-H. Leung and D.-L. Ma, *Sens. Actuators, B*, 2017, **243**, 971-976.
10 D.-L. Ma, M. Wang, C. Liu, X. Miao, T.-S. Kang and C.-H. Leung, *Coord. Chem. Rev.*, 2016, **324**, 90-105.
11 H.-C. Zhou, J. R. Long and O. M. Yaghi, *Chem. Rev.*, 2012, **112**, 673-674.
12 S. Rojas, T. Devic and P. Horcajada, *J. Mater. Chem. B*, 2017, **5**, 2560-2573.
13 P. Horcajada, C. Serre, M. Vallet□Regí, M. Sebban, F. Taulelle and G. Férey, *Angew. Chem.*, 2006, **118**, 6120-6124.
14 P. Horcajada, R. Gref, T. Baati, P. K. Allan, G. Maurin, P. Couvreur, G. Férey, R. E. Morris and C. Serre, *Chem. Rev.*, 2011, **112**, 1232-1268.
15 P. Horcajada, C. Serre, G. Maurin, N. A. Ramsahye, F. Balas, M. Vallet-Regí, M. Sebban, F. Taulelle and G. Férey, *J. Am. Chem. Soc.*, 2008, **130**, 6774-6780.
16 J. An, S. J. Geib and N. L. Rosi, *J. Am. Chem. Soc.*, 2009, **131**, 8376-8377.
17 P. Horcajada, T. Chalati, C. Serre, B. Gillet, C. Sebrie, T. Baati, J. F. Eubank, D. Heurtaux, P. Clayette and C. Kreuz, *Nat. Mater.*, 2010, **9**, 172-178.
18 R. Anand, F. Borghi, F. Manoli, I. Manet, V. Agostoni, P. Reschiglian, R. Gref and S. Monti, *J. Phys. Chem. B*, 2014, **118**, 8532-8539.
19 C.-Y. Sun, C. Qin, X.-L. Wang, G.-S. Yang, K.-Z. Shao, Y.-Q. Lan, Z.-M. Su, P. Huang, C.-G. Wang and E.-B. Wang, *Dalton Trans.*, 2012, **41**, 6906-6909.
20 C. Y. Sun, C. Qin, C. G. Wang, Z. M. Su, S. Wang, X. L. Wang, G. S. Yang, K. Z. Shao, Y. Q. Lan and E. B. Wang, *Adv. Mater.*, 2011, **23**, 5629-5632.
21 F. R. S. Lucena, L. C. de Araújo, M. d. D. Rodrigues, T. G. da Silva, V. R. Pereira, G. C. Militão, D. A. Fontes, P. J. Rolim-Neto, F. F. da Silva and S. C. Nascimento, *Biomed. Pharmacother.*, 2013, **67**, 707-713.
22 W. Lin, Q. Hu, K. Jiang, Y. Yang, Y. Yang, Y. Cui and G. Qian, *J. Solid State Chem.*, 2016, **237**, 307-312.
23 W. Lin, Q. Hu, J. Yu, K. Jiang, Y. Yang, S. Xiang, Y. Cui, Y. Yang, Z. Wang and G. Qian, *ChemPlusChem*, 2016, **81**, 804-810.
24 S. Rojas, P. S. Wheatley, E. Quartapelle-Procopio, B. Gil, B. Marszalek, R. E. Morris and E. Barea, *CrystEngComm*, 2013, **15**, 9364-9367.
25 A. C. McKinlay, P. K. Allan, C. L. Renouf, M. J. Duncan, P. S. Wheatley, S. J. Warrender, D. Dawson, S. E. Ashbrook, B. Gil and B. Marszalek, *APL Mater.*, 2014, **2**, 124108-124116.
26 R. Babarao and J. Jiang, *J. Phys. Chem. C*, 2009, **113**, 18287-18291.
27 L. Bei, L. Yuanhui, L. Zhi and C. Guangjin, *Acta Chim. Sinica*, 2014, **72**, 942-948.

28 M. C. Bernini, D. Fairen-Jimenez, M. Pasinetti, A. J. Ramirez-Pastor and R. Q. Snurr, *J. Mater. Chem. B*, 2014, **2**, 766-774.
29 R. Bueno-Perez, A. Martin-Calvo, P. Gomez-Alvarez, J. J. Gutierrez-Sevillano, P. J. Merkling, T. J. H. Vlugt, T. S. van Erp, D. Dubbeldam and S. Calero, *Chem. Commun.*, 2014, **50**, 10849-10852.
30 I. Erucar and S. Keskin, *Ind. Eng. Chem. Res.*, 2016, **55**, 1929-1939.
31 M. Kotzabasaki, I. Galdadas, E. Tylianakis, E. Klontzas, Z. Cournia and G. E. Froudakis, *J. Mater. Chem. B*, 2017, **5**, 3277-3282.
32 Y. Xin, T. Hu and P. K. Chu, *Acta Biomater.*, 2011, **7**, 1452-1459.
33 R. T. Greenlee, T. Murray, S. Bolden and P. A. Wingo, *Ca-Cancer J. Clin.*, 2000, **50**, 7-33.
34 J. Wang, J. Jin, F. Li, B. Li, J. Liu, J. Jin, C. Wang, Y. Zeng and Y. Wang, *RSC Adv.*, 2015, **5**, 85606-85612.
35 C. Gu, F. Li, B. Li, J. Xu, S. Yang, M. Luo, J. Liu and G. Liu, *Inorg. Chem. Commun.*, 2016, **73**, 26-29.
36 C.-Y. Sun, C. Qin, X.-L. Wang, G.-S. Yang, K.-Z. Shao, Y.-Q. Lan, Z.-M. Su, P. Huang, C.-G. Wang and E.-B. Wang, *Dalton Trans.*, 2012, **41**, 6906-6909.
37 F. R. S. Lucena, L. C. de Araújo, M. d. D. Rodrigues, T. G. da Silva, V. R. Pereira, G. C. Militão, D. A. Fontes, P. J. Rolim-Neto, F. F. da Silva and S. C. Nascimento, *Biomed. Pharmacother.*, 2013, **67**, 707-713.
38 F. H. Allen, *Acta Crystallogr., Sect. B: Struct. Sci.*, 2002, **58**, 380-388.
39 H. Deng, S. Grunder, K. E. Cordova, C. Valente, H. Furukawa, M. Hmadeh, F. Gándara, A. C. Whalley, Z. Liu and S. Asahina, *Science*, 2012, **336**, 1018-1023.
40 T. F. Willems, C. H. Rycroft, M. Kazi, J. C. Meza and M. Haranczyk, *Microporous Mesoporous Mater.*, 2012, **149**, 134-141.
41 Materials Studio v8.0. Biovia Software Inc., CA 92121,USA.
42 E. E. Bolton, Y. Wang, P. A. Thiessen and S. H. Bryant, *Annu. Rep. Comput. Chem.*, 2008, **4**, 217-241.
43 A. K. Rappe, C. J. Casewit, K. S. Colwell, W. A. Goddard and W. M. Skiff, *J. Am. Chem. Soc.*, 1992, **114**, 10024-10035.
44 C. E. Wilmer, K. C. Kim and R. Q. Snurr, *J. Phys. Chem. Lett.*, 2012, **3**, 2506-2511.
45 D. Frenkel and B. Smit, *Understanding Molecular Simulation: From Algorithms to Applications*, Elsevier Science, 2001.
46 Y. G. Chung, J. Camp, M. Haranczyk, B. J. Sikora, W. Bury, V. Krungleviciute, T. Yildirim, O. K. Farha, D. S. Sholl and R. Q. Snurr, *Chem. Mater.*, 2014, **26**, 6185-6192.
47 L. B. de Oliveira Freitas, I. J. G. Bravo, W. A. de Almeida Macedo and E. M. B. de Sousa, *J. Sol-Gel Sci. Technol.*, 2016, **77**, 186-204.
48 A. Singh, N. Thotakura, R. Kumar, B. Singh, G. Sharma, O. P. Katare and K. Raza, *Int. J. Biol. Macromol.*, 2017, **95**, 750-756.
49 J. Wu, A. Deng, W. Jiang, R. Tian and Y. Shen, *Mater. Sci. Eng. C*, 2017, **71**, 132-140.
50 R. A. Al-Thawabeia and H. A. Hodali, *J. Chem.*, 2015, **2015**.
51 Z. Jianping, G. Jianfeng, Z. Yao and Y. Jiao, *J. Biomater. Sci., Polym. Ed.*, 2014, **25**, 1828-1841.